energies

IMPACT FACTOR 3.2

CITESCORE 5.5

Article

Cavitation Hydrodynamic Performance of 3-D Printed Highly Skewed Stainless Steel Tidal Turbine Rotors

Stylianos Argyrios Pitsikoulis, Sravya Tekumalla, Anurag Sharma, Wai Leong Eugene Wong, Serkan Turkmen and Pengfei Liu

MDPI

https://doi.org/10.3390/en16093675

energies

MDPI

Article

Cavitation Hydrodynamic Performance of 3-D Printed Highly Skewed Stainless Steel Tidal Turbine Rotors

Stylianos Argyrios Pitsikoulis [1], Sravya Tekumalla [2,3], Anurag Sharma [4], Wai Leong Eugene Wong [5], Serkan Turkmen [1] and Pengfei Liu [1,*]

[1] School of Engineering, Newcastle University, Newcastle upon Tyne NE1 7RU, UK
[2] School of Mechanical and Aerospace Engineering, Nanyang Technological University, Singapore 639798, Singapore
[3] Department of Mechanical Engineering, University of Victoria, Victoria, BC V8W 2Y2, Canada
[4] School of Electrical and Electronic Engineering, Newcastle University in Singapore, 172A Ang Mo Kio Avenue 8 #05-01, Singapore 567739, Singapore
[5] School of Mechanical and Systems Engineering, Newcastle University International Singapore, 180 Ang Mo Kio Avenue 8, Singapore 569830, Singapore
* Correspondence: pengfei.liu@newcastle.ac.uk

Abstract: Hydraulic turbines contribute to 60% of renewable energy in the world; however, they also entail some adverse effects on the aquatic ecology system. One such effect is their excessive noise and vibration. To minimize this effect, one of the most effective and feasible solutions is to modify the design of the turbine rotor blade by introducing a skew. In this study, two 0.3-meter tidal turbines with 0-degree (no-skewness) and positive 90-degree skewness made of stainless steel 316L were designed and printed using a 3-D printing powder bed fusion technique. These rotors were then tested at the Emerson Cavitation Tunnel (ECT) at Newcastle University, UK, and the variation in the skewness of the blades of the turbines as a function of the power coefficient on a given tip speed ratio (TSR) value was ascertained. Results showed that the highly skewed rotor had significantly lower drag and torque fluctuations, with a slight decrease in efficiency compared to the non-skewed one, which warrants further investigation on the effect of added skew to reduce vibration and noise. Numerical simulations were also performed for verification and validation of the experimental tests, using the H45 dynamometer at the ECT. A comprehensive software code for propellers and tidal turbines, ROTORYSICS, was used to examine the cavitation effect of the two rotors; a comparison was made for both, with and without cavitation. The results indicate that for a high immersion depth of tidal turbine rotors, cavitation rarely occurs, but for hydrokinetic turbines that are installed on dams in rivers and falls, cavitation could be a serious concern. It was concluded that the 0-degree skewed rotor is more hydrodynamically efficient than the 90-degree skewed rotor.

Keywords: tidal turbines; cavitation tunnel; cavitation; blade skewness; power generation; structural integrity; environmental impact

Citation: Pitsikoulis, S.A.; Tekumalla, S.; Sharma, A.; Wong, W.L.E.; Turkmen, S.; Liu, P. Cavitation Hydrodynamic Performance of 3-D Printed Highly Skewed Stainless Steel Tidal Turbine Rotors. *Energies* **2023**, *16*, 3675. https://doi.org/10.3390/en16093675

Academic Editor: Mohamed Benbouzid

Received: 22 March 2023
Revised: 6 April 2023
Accepted: 10 April 2023
Published: 25 April 2023

1. Introduction

Due to increased CO_2 levels around the world, some countries, especially the UK, have decided to implement a strategy to decrease carbon levels in the power sector so that a net-zero emission target by 2050 can be attained, and ultimately reduce their contribution to global warming within 30 years. Emissions of CO_2 and other harmful gases that are a product of fossil fuel combustion contribute to the effects of climate change even more; combined with the continuous increase in fuel prices, this has led many researchers to find alternative ways of energy generation from renewable resources [1,2].

Tidal turbines contribute to 60% of global renewable energy production. However, they are also responsible for some negative environmental effects, due to the disturbances formed around the rotors which, in their turning, create noise and vibration. This effect

can be mostly observed in ship propellers, as cavitation is the source of vibration and noise which, apart from propulsive losses, is responsible for threatening marine life, especially to noise-sensitive animals [3,4]. Equipping a whole coastal area with tidal turbines can be catastrophic for the whole ecosystem, and reduce their energy production efficiency due to disturbances from each other. Kumar et al. (2022) [5] presented an experimental study for a wheel-type tidal turbine with a slight blade skew and several different endplates to reduce the noise.

The main challenge with tidal turbines is to enhance their energy production capabilities so that they can be as competitive as other renewable energy resources [6] in addition to enabling them to operate with minimized vibration and noise under extreme environmental conditions. Accurately predicting the mechanical loads the tidal turbines are subjected to due to turbulence can be quite challenging and potentially catastrophic, if not calculated precisely before their installation; this ultimately what determines their "lifespan" [7]. Despite advancements in engineering in the past 15 years, marine renewable technology is still not on par with wind and solar power, mainly due to the complexity of their design and installation.

While very few studies on highly skewed blades of tidal turbine rotors are available, there are many studies on propeller skew effect on aero- and hydrodynamics performance. Among many publications, Asnaghi (2018) [8] addressed propeller skew effect on hydrodynamic performance and acoustic noise. Some studies in this category include Tong et al. (2021) [9], on ingesting inflow turbulence. Ebrahimi (2021) [10] concluded a testing program for a traditional B-series propeller on cavitation and noise. Yu et al. [11] presented their study on the skew effect on propulsive performance and noise for a submarine propeller. Hadipour (2021) [12] conducted research on the effect on performance and noise of seven highly skewed propellers in nonuniform inflow. Lippert (2012) [13] developed a numerical model to simulate underwater turbine noise levels, but did not link the skew effect to the noise. Muller and Pecot (2017) [14] developed a fluid structure coupling for composite tidal turbines, with a much smaller skew of up to 15 degrees.

Starzmann et al. (2014) [15] discussed the blade skew effect of aerodynamic performance linked with noise on the Wells turbine for turbomachinery.

In terms of cavitation, there are numerous studies in the literature, especially cavitation effects on the hydrocyanic performance of rotors. Ge et al. [16,17] presented a recent study on cavitation coupled with thermodynamic effects, and hydrodynamic cavitation performance in Venturi-type reactors, respectively.

There have been attempts to improve the technological capabilities of tidal turbines; however, there are limited data available on the operating conditions of tidal turbines for a thorough study [18]. Another aspect of the challenge is the site of operation of the tidal turbines, which affects the performance of the equipment since there are different flow conditions depending on the site; this makes the problem situational [19].

Along with reliable computational fluid dynamics (CFD) simulations, model testing has proved to be quite accurate in predicting the performance of such equipment, and has provided promising results. In this research, the design challenges of these turbines were overcome using a 3-dimensional (3-D) printing technique to produce two stainless steel 316L-based tidal turbine rotor models. Metal 3-D printing techniques, such as laser powder bed fusion (LPBF), offer new possibilities and freedom to design parts with complex geometries, controlled porosities, and tailored properties. Using the LPBF technique, 0-degree and 90-degree skews were introduced in the turbines, and the effect of blade skew on cavitation and the overall performance of the tidal turbine rotors was ascertained by conducting experimental tests at the ECT at Newcastle University. A comparative analysis for the two rotors is provided on the design of the turbines (in terms of efficiency and strength. The ocean environment that turbines operate in is harsh, posing the biggest risk factor in terms of failure [20]), and impacts turbines' effects on aquatic life and the environment.

2. Research Methods

In this section, the necessary equipment and apparatus that were used to carry out the experiments for data acquisition are presented, along with the characteristics of the cavitation tunnel.

2.1. Tidal Turbines

For this study, two tidal turbines (Figure 1) were prototyped and designed [21]. They were 3-D printed using the LPBF technique on a MetalFABG2 printer in Singapore, which has a powder bed size of 420 × 420 × 400 mm^3 (L × W × H) and is equipped with 4 fiber lasers, each with a wavelength between 1078 nm and 1082 nm, and a spot size of 105 µm. During the printing process, a layer of 50 µm in thickness and a zig-zag scan strategy (stripe width: 10 mm) with an incremental scan rotation of 67 degrees for each layer was used, with an overall volumetric energy density set to 52 J/mm^3. The printed parts are shown in Figure 1. Due to the complexity in the design of the turbines, porous block support structures (generated on Magics software) were also used during printing. Following the printing process, post processing heat treatment was carried out to relieve the rotors of any residual stresses. The rotors were heated to 1050 °C at a rate of 8 °C/min in an argon atmosphere, held for 30 min, and quenched to room temperature. After the stress-relieving treatment, the rotors were wire-cut from the substrates, the support structures were removed, and N4 surface finishing treatment was carried out on the rotors before further testing.

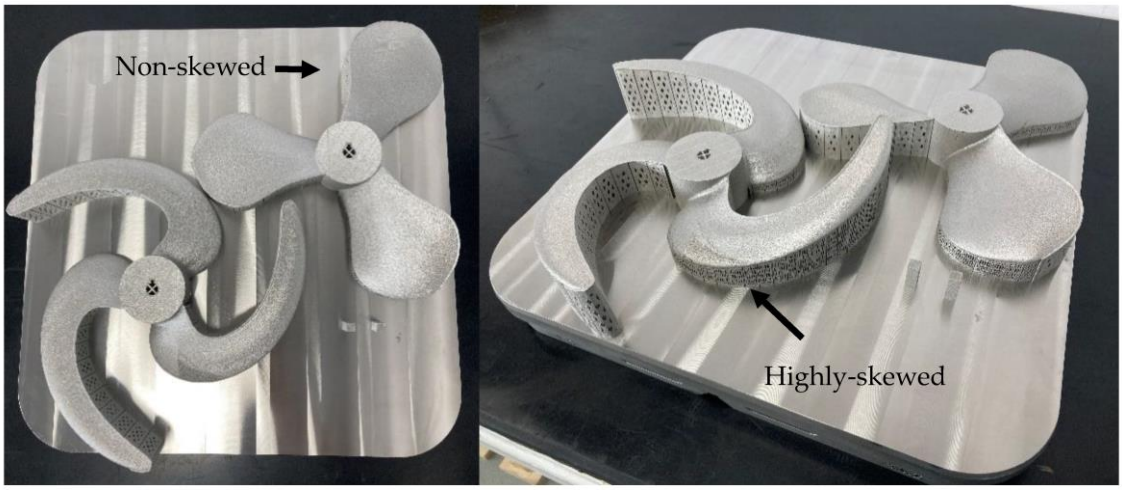

Figure 1. 3-D printed highly skewed tidal turbine (**right**) and non-skewed tidal turbine (**left**) used in this study.

Both tidal turbines shared the same main dimensions and characteristics, which can be seen in Table 1 below.

Table 1. Main dimensions of the tidal turbines.

Turbine Particulars		
Diameter	300 mm	
No. of Blades	3	
Pitch	0.51	
Skew angle	0	+90
Material	Stainless steel 316L	

2.2. The Cavitation Tunnel

The experiments required for the data acquisition of this study were conducted in the ECT, which is part of Newcastle Upon Tyne University based in Blyth. Inside the cavitation tunnel, water is circulated by an impeller that runs in the vertical plane, simulating the flow of water. Different testing scenarios can be simulated by adjusting the flow speed of the water, the rotational speed of the shaft, the immersion depth of the shaft and the pressure inside the tunnel to replicate the actual operating conditions. Note that it was impossible to achieve 100% accurate simulation of the actual full-scale flow field, because of Reynolds number and Froude number similarity.

Over the years, the cavitation tunnel has undergone many modifications until its present form, serving as an ideal facility for the cavitation testing of model propellers and tidal turbines in a range of 150 mm to 400 mm in diameter. A windowed test section located at the upper side of the tunnel, with dimensions of 3100 mm × 1219 mm × 806 mm (L × B × H), allows for observations inside the tunnel. Moreover, photos and videos of the environment inside the testing window can be captured with the aid of a strobe light and a camera, which are connected to a monitor to provide real-time feedback.

Experiment Equipment and Apparatus

A Kempf & Remmers H45 type dynamometer assembly fitting was contained within the pod where the turbine was mounted, as shown in Figure 2. This dynamometer is suitable for testing model propellers and turbines with a maximum diameter of 400 mm.

Figure 2. Kempf & Remmers H45 torpedo-shaped fitting with 0 degrees of skewness tidal turbine mounted.

The dynamometer has capabilities of measuring the blade forces of controllable pitch propellers, using slip rings that are fitted inside the dynamometer which transmit signals from a hub dynamometer. The capabilities of the H45 type dynamometer, as of the day of the experiments, were the following:

- Maximum shaft RPM: 2750;
- Maximum thrust: ±2750 N;
- Maximum torque: ±135 Nm.

In Figure 3, a part of the control panel is shown where real-time information regarding the environment inside the cavitation tunnel can be observed. For the experiments, the following features of this panel were used:

- The RPM reader where the shaft revolution speed was measured;
- The amplifiers for receiving the signal of thrust and torque inside the testing window;
- The button to reset the amplifiers at the beginning of each test;

- The buttons which allow switching between the thrust and torque amplifiers.

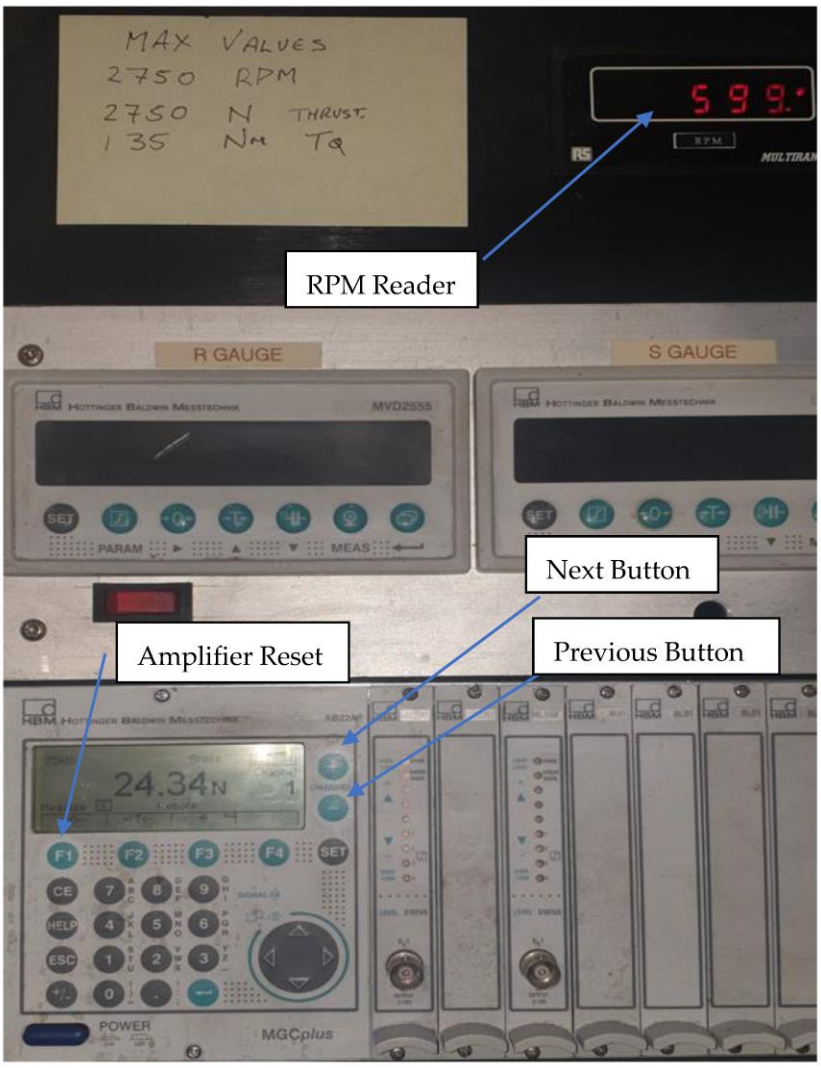

Figure 3. Dynamometer and shaft output values.

The environment inside the cavitation tunnel was controlled, using the control panel as seen in Figure 4. For the experiments, the following features were used:

- The impeller speed dial that controls the inflow velocity of the water inside the tunnel;
- The shaft rotational speed dial that controls the RPM of the shaft;
- The valves that are used to apply a vacuum inside the cavitation tunnel, which is mainly used during cavitation tests.

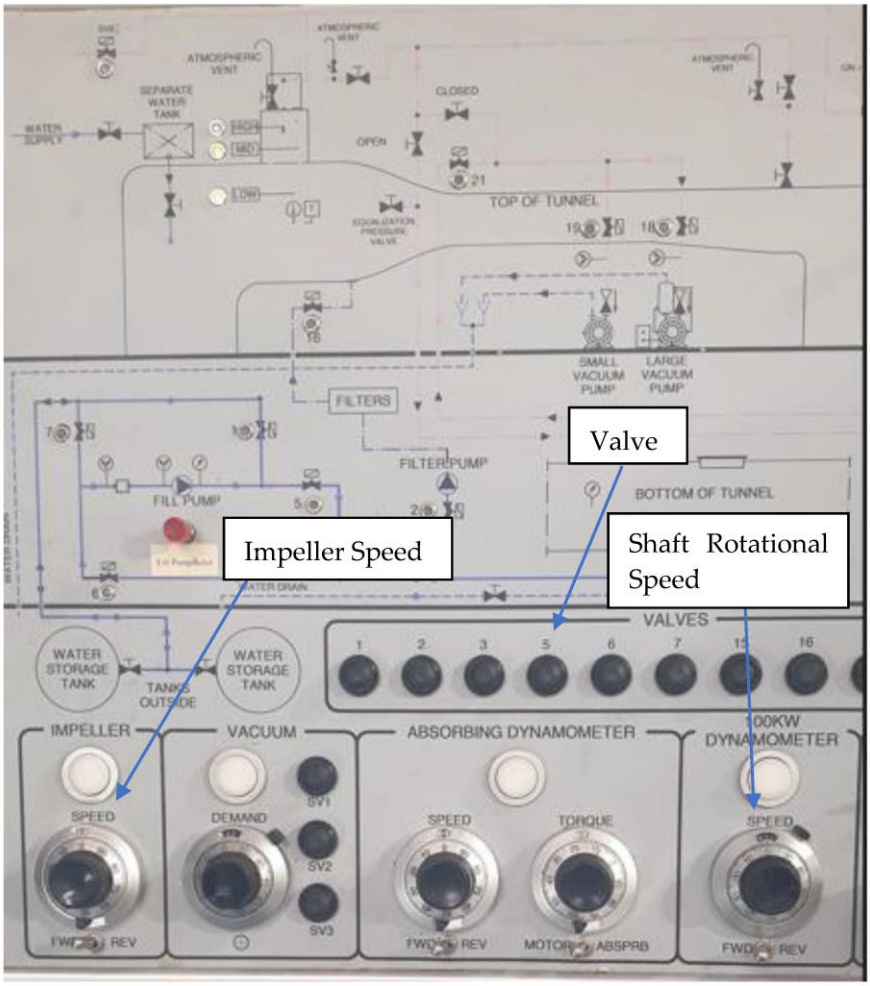

Figure 4. Cavitation tunnel controls.

3. Results and Discussion

In this section, the results of the open water tests performed for the 0 degrees and 90 degrees skew tidal turbine are presented. The same experimental testing procedure and test matrix for the open water test was used in the previous study [21]; however, in this research, instead of a towing tank, a cavitation tunnel was used to examine the effect of fabrication on the hydrodynamic characteristics of tidal turbines with identical geometries and the same testing parameters, i.e., the effect of metal 3-D printing/additive manufacturing on the hydrodynamic performance of the tidal turbines. In addition, using the ECT, the cavitation characteristics of the turbine rotors were also examined.

The effect of skew on power production performance is presented in Figure 5. In Figure 5, the trend of the power coefficient, i.e., C_{pow} for a given TSR, is shown, which indicates the results that were obtained from the open water tests. The trends of the curves produced from the experiments for the same TSR should agree, though the magnitude could be slightly different. It can be seen that the blade with no skew had a much higher power production efficiency than the blade with a very large skew of 90 degrees.

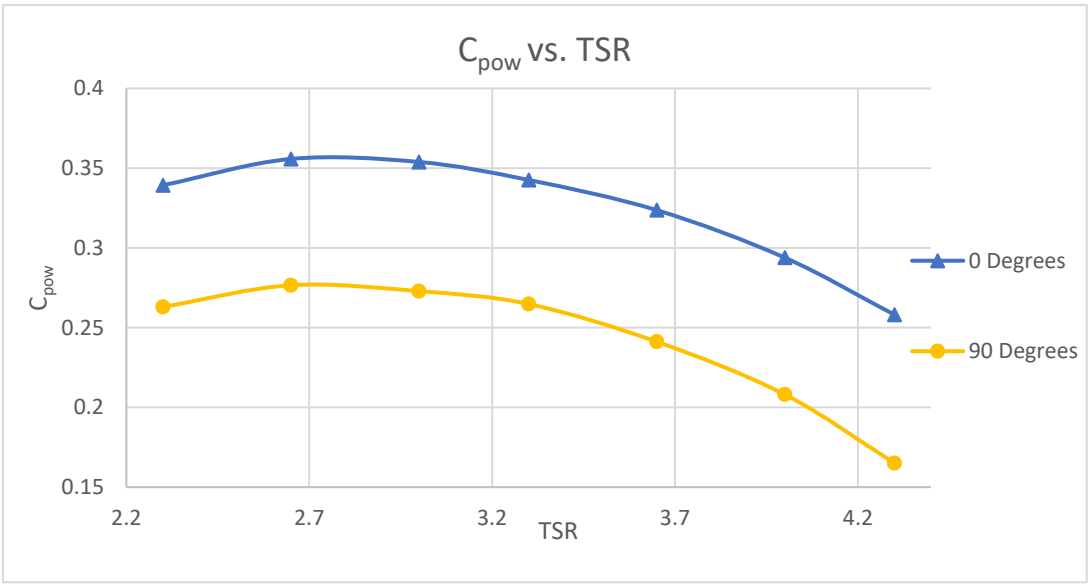

Figure 5. C_{pow} vs. TSR for 0- and 90-degree skewed tidal turbines [21].

3.1. Experimental Open Water Testing

Before the actual experimental testing, an open water test was performed to confirm whether the cavitation tunnel was in good condition and the results obtained were valid.

For this reason, a test matrix was created specifically for the open water test, where for a fixed shaft speed, the inflow velocity was to be adjusted to obtain the same TSR value for each open water test in a range from 2.3 up to 4.3 TSR.

By obtaining the C_{pow} for each set and plotting them together on the same graph, the resulting curves for C_{pow} against TSR should almost coincide, or have minimal difference due to the effect of the Reynolds number.

As seen in Figure 6, the resulting curves do not agree with each other, except for tests No.4 and No.5, which follow the same trend. The reason behind the abnormal trend of the first three curves could be the low RPM values used during the experiments, which were not enough for the dynamometer to accurately register. As the maximum capability of the dynamometer for torque measurements is around ±135 Nm, obtaining less than 1% of the maximum value may add substantially more uncertainty.

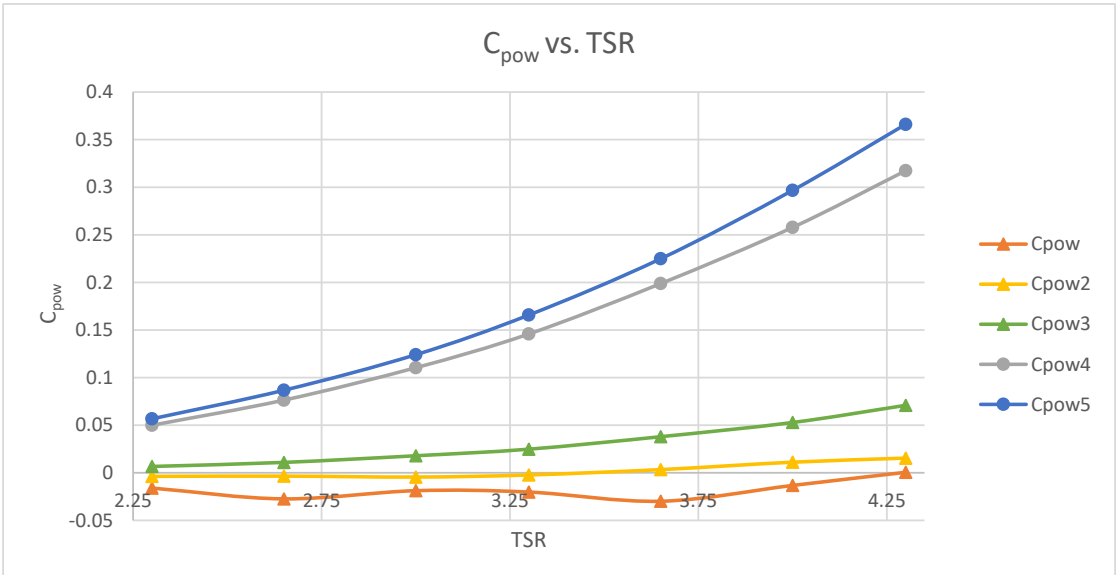

Figure 6. Open water test results for C_{pow} vs. TSR.

3.1.1. Comparison with AMC Towing Tank Experimental Test

In this part, the same test matrix used previously [21] at the AMC towing tank was followed and repeated this time in the cavitation tunnel, in order to test the effect of 3-D printed materials on hydrodynamic performance.

Owing to the discrepancies in the experimental results and inaccuracies as shown in Appendix B: Figure A2, efforts were made to repeat the tests numerous times to confirm whether the fault was human error or dynamometer malfunction. Through trial and error, the problem identified was due to the sensitivity and instability of the dynamometer, which was partly due to the output torque value being too small to be accurately registered.

Therefore, an attempt was made to modify the test matrix and increase the torque to produce more accurate results that the dynamometer could "read". In doing so, the C_{pow} curve should be close to the one obtained from the previous experiments conducted by Foong (2019) [21], since the new combination of shaft rotational speed and inflow velocity would result in the same TSR values for each test run.

3.1.2. Modification of Test Matrix Based on Previous Test Observations

As mentioned in Section 3.1.1, an attempt was made to produce more meaningful results by eliminating the thus far identified problem of the dynamometer detecting very low torque values compared to its maximum capability.

Assuming that the main cause of the wrong results was dynamometer sensitivity, then increasing the torque would theoretically eliminate the problem. Thus, the previous test matrix was modified accordingly by doubling the rps, n, ($n' = 2n$) and inflow velocity ($V_a' = 2V_a$) to maintain the same TSR for each test run.

The new test matrix produced torque values far more than 1% of the maximum torque capability of the dynamometer, and the difference between the previous tests and the new modified test matrix was evident. The trend of the curve became closer to the ideal one; by repeating the test run a second time to confirm consistency between the data, the curves almost coincided with each other for relatively high torque values. However, the measured torques values at the higher TSR (lower inflow speeds) were still unstable, as shown in Figure 7, for TSR values higher than 3.3.

Figure 7. Test run 12 and test run 13, C_{pow} vs. TSR comparison.

The resulting curves for C_{pow} from the new modified test matrix were quite promising, although there was still room for improvement. This discrepancy may also be attributed to the effect of the 3-D printed material on hydrodynamic performance. The trend of the

curve was almost as perfect as expected (as seen from the AMC curve produced in the towing tank shown in Figure 8), but the error between them was relatively large, indicating that there was a problem with the current H45 dyno in mission.

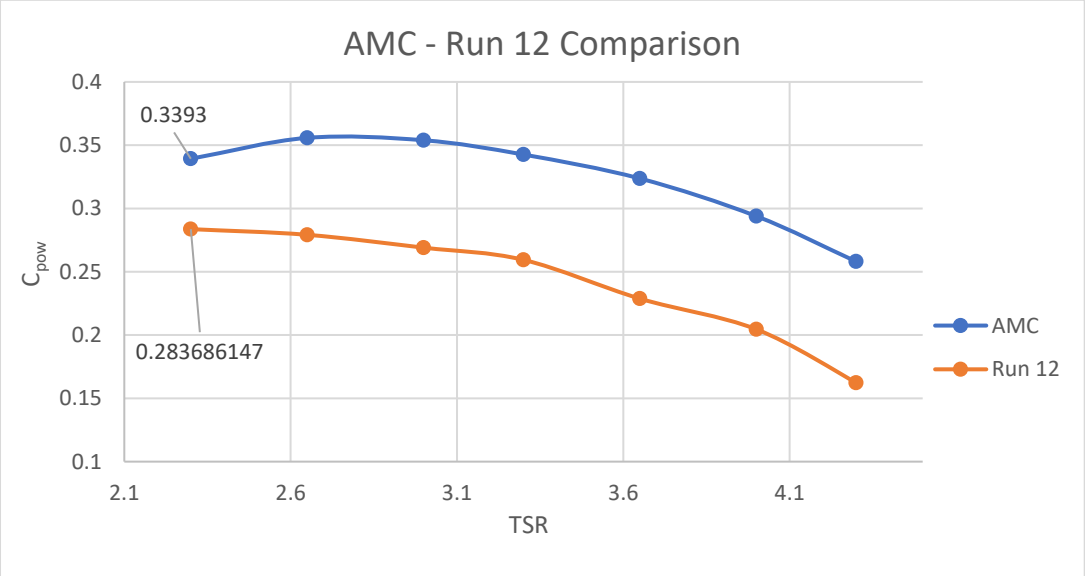

Figure 8. AMC and test run 12, C_{pow} vs. TSR comparison.

For example, the error between the first values of the data set from AMC and test run 12 was as follows:

$$Error\ \% \approx (0.3393 - 0.2837) \times 100\% \approx 5.56\%$$

Having a $\approx$ 5.56% error between the two data sets was acceptable, but still not quite satisfactory. Thus, the test matrix was further modified, based on maximizing the output torque.

3.1.3. Finalization of Test Matrix

Having the maximum capability of inflow velocity of the cavitation tunnel in mind (6.05 m/s), the rps and inflow velocity were multiplied by 2.5, which is the limit to not exceed the capabilities of the cavitation tunnel.

Further increasing the torque as much as possible resulted in a curve with the ideal trend and smoothness. Moreover, by repeating the same test run, the resulting curves almost coincided with each other (Figure 9), eliminating any error and inconsistency between them; this indicated that for high torque values, the tests were meaningful.

However, upon comparing the results with the ones obtained in the AMC towing tank, although the curves improved, they still did not coincide with each other in terms of magnitude. This may be attributed to the different of turbine materials (current stainless vs. previous plastic) and the optimum pitch values. For stainless steel materials, the optimum pitch may need to be re-optimized.

Figure 10 shows the power coefficient of the plastic rotor obtained at AMC [21] and the power coefficient of the stainless-steel rotor obtained at the ECT at Newcastle University.

Figure 9. Test run 16 and test run 17 comparison.

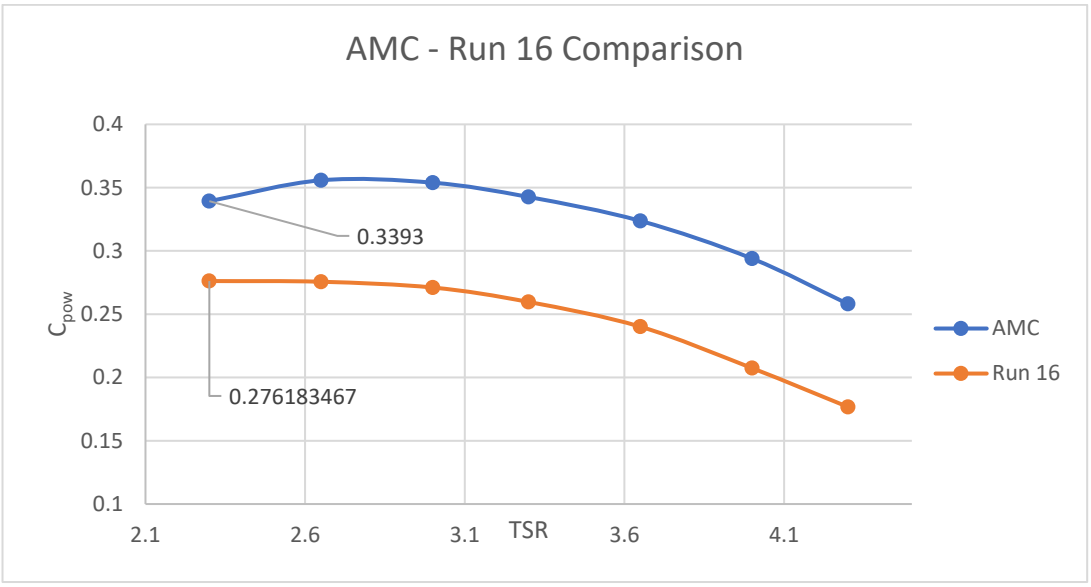

Figure 10. AMC and test run 16 comparison.

Despite the curves following the same trend, they still had a large error in their magnitude, indicating that apart from the capacity problem of the dynamometer, another variable of the dynamometer was causing further inaccuracies.

For example, the error between the first values of the data set from Foong's (2019) [21] test run 12 was the following:

$$Error\ \% \approx (0.3393 - 0.2762) \times 100\% \approx 6.31\%$$

Once again, the discrepancy seemed large, though part of the discrepancy could be attributed to the effect of the type of 3-D printed material on hydrodynamic performance, i.e., the material in the previous study was 3-D printed plastic, and the current study's material was 3-D printed stainless steel 316L.

3.2. Attempts towards Equipment Fault Identification

Numerous additional tests were performed to isolate the fault on the H45 dyno even further. For example, the tip speed ratio value was kept constant for three different test runs while multiplying the original shaft revolutions per second value by a constant number. For that TSR value, the resulting curves should follow the same trend, which, as seen in Appendix B: Figure A1, they did not. Finally, by keeping the RPM constant at 600, 720 and 840, and varying the inflow velocity for a set of test runs, the following example test matrix and curves were produced (as shown in Figure 11):

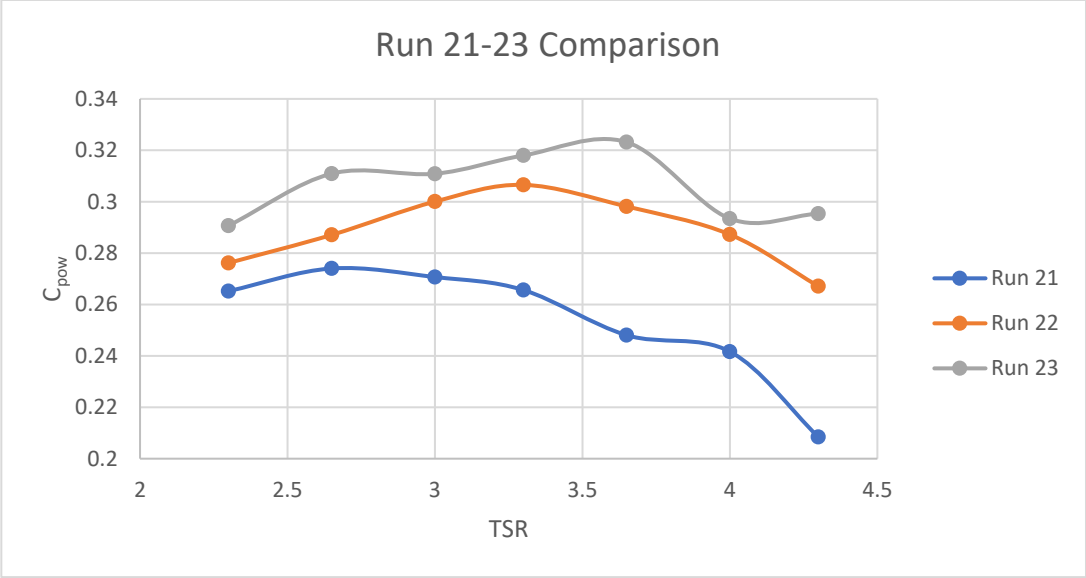

Figure 11. Test runs 21, 22 and 23, comparison at constant RPM.

The curves were once again quite inconsistent, without any of them following a trend. Since the shaft speed rps of each data set was kept constant, the problem could have occurred due to inconsistent inflow speed. Even though the inflow velocity was controlled from the inflow velocity dial on the control panel, it would still not be possible to determine whether the actual inflow velocity was the same as the one set from the dial, as there was no sensor inside the testing window of the cavitation tunnel. Thus, it could not be concluded with certainty whether the problem occurred due to the inflow speed, since there was no means of estimating the real value inside the tunnel to confirm its inaccuracy.

We came up a feasible way to eliminate this problem, which was to keep the inflow speed constant for each test and vary the shaft speed rps or RPM; however, the whole point of the tests was to repeat the same test conditions as the ones performed at the AMC towing tank and achieve the same results.

However, in doing so, the effects of the Reynolds number on the thrust/drag and power coefficients needed to be considered. In a study conducted based on CFD analysis and experimental testing on the effects of Reynolds number on the thrust and torque coefficients of a propeller [22], it was confirmed that for the same advance coefficient J value (in the case of tidal turbines, TSR), at different RPM values, the resulting curves of the coefficients should follow the same trend, with the only difference due to the Reynolds number effect.

Although keeping the inflow speed constant and changing the shaft speed to achieve the target TSR values is much more efficient to operate the tunnel, it is not a recommended testing operation. The reason that shaft speed needs to be fixed, and to vary the inflow speed to obtain the desired TSR values, is to keep a relatively constant Reynolds number for a series of tests for all the data points of C_T and C_{pow}, according to the ITTC—open water test procedure in Section 3.3.4 of the ITTC document [23,24].

3.2.1. Zero-Degree Skewed Tidal Turbine Cavitation Test

Bearing in mind the error produced during the open water tests and the unsatisfactory results, a cavitation test was performed based on the test matrix and parameters that produced the best curves, in spite of the error in the magnitude of the power coefficient. Regardless of the error in the magnitude of the power coefficient, ideally, the cavitation test results should be adequate based on the trend of the curves. Figure 12 shows the tip vortex cavitation of a typical cavitation test for the zero-skew rotor.

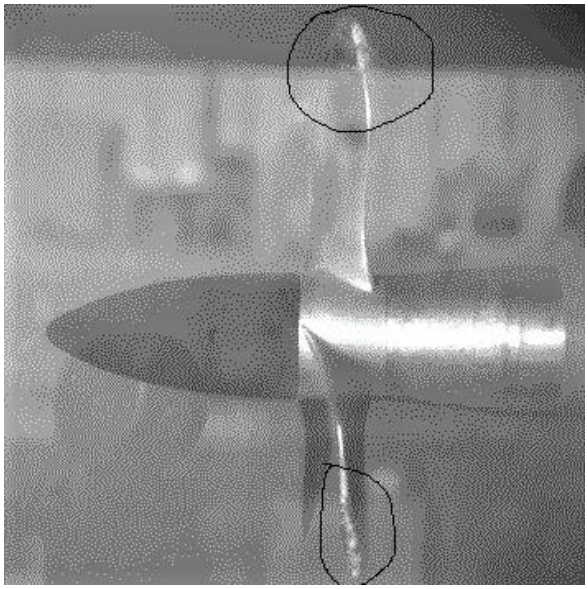

Figure 12. Zero-degree skewed tidal turbine tip cavitation. The tip cavitation is circled in the figure.

The procedure for the cavitation tests is summarized below. The vacuum was applied inside the cavitation tunnel through the suitable valves to reduce the pressure inside the tunnel. Then, after 20–30 min, the concentration of mmHg, whose range was maintained between 400–800 mmHg, would be high enough to achieve a lower cavitation number (the least possible). Upon reaching the desired mmHg value, the test parameters for inflow speed and shaft speed RPM were fixed, and then the mmHg concentration in the tunnel began to drop sharply, which allowed a small window for recording the data for low cavitation numbers. For this reason, the same test was repeated three times to collect the data for each cavitation number of the test matrix. It was crucial to ensure that the cavitation tunnel was operated at a medium shaft rotational speed (around 500 RPM) for at least 20 min before experimental testing, in order for the dynamometer to "warm up". If the aforementioned advice is not followed, the results from the tests will be random and meaningless. Moreover, after each test, it must be ensured that the thrust and torque amplifiers are reset after the dynamometer and inflow speed dial have been turned off, to avoid disturbances in the data.

The governing equations that were used to produce the necessary test matrix for cavitation testing are the following:

$$P_{shaft} = P_{atm} + \rho g H \tag{1}$$

$$P_{dynamic} = 0.5 \times \rho \times n^2 \times D^2 \tag{2}$$

$$P_{tunnel} = \sigma_n \times P_{dynamic} + P_{vapor} - P_{Shaft} \tag{3}$$

$$\sigma_n = \frac{P_{shaft} - P_{vapor}}{0.5\rho n^2 D^2} \quad (4)$$

where:

- $P_{atm} = 101{,}300$ Pa;
- $H = 0.4$ m;
- $P_{vapor} = 1931.51$ Pa, calculated through linear interpolation based on the water temperature of the day that the tests were conducted, which was $T = 17.1$ °C.

The problem of the non-ideal curve could be avoided by operating the impeller at higher TSR, which is not demanding in terms of inflow speed and RPM; however, since the output torque was low (around 3 Nm), the results were not accurate, and there was no point in further testing.

An attempt was made to increase the cavitation number to avoid such inconsistencies, since, for a higher cavitation number, a lower concentration of mmHg in the tunnel was needed. By slightly increasing the cavitation number, even from a minimum of σ_n = 1 to a σ_n = 2.5, such problems were avoided, without any significant impact in the long term because tidal turbines operate in relatively high cavitation numbers. Figure 13 shows the power coefficient of the zero-skew rotor at a TSR of 2.3.

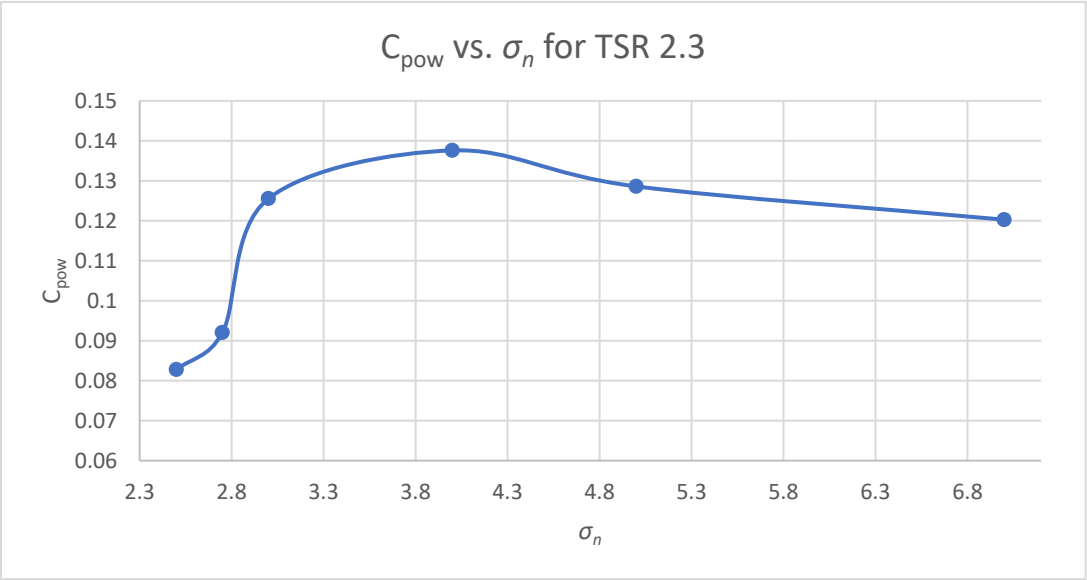

Figure 13. C_{pow} vs. σ_n for TSR = 2.3.

The curve produced from the cavitation test at TSR = 2.3 resembles the expected trend of an ideal curve, but is inconsistent. The curve indicates that at relatively high σ_n values (around 4), the performance is optimal until it starts dropping for even higher cavitation numbers. However, since there were no more tests conducted for different TSR values, it was impossible to validate these data without obtaining more experimental data.

3.2.2. 102 Series Propeller Open Water Test

In a final attempt to determine the condition of the cavitation tunnel, further open water tests were conducted, this time using the 102 series propeller (Figure 14), which is a stock propeller at the ECT. The purpose of this test was to confirm whether the current H45 dynamometer was unreliable and unstable.

Figure 14. Mounted 102 series propeller.

Since there were already existing data from experimental tests conducted over 40 years ago on the same propeller when the equipment was in its optimum state, the present condition of the dynamometer was determined by comparing the past experimental data with the new experimental data; a test matrix was created with the same operating conditions. The following are the characteristics of the 102 series propeller (see Table 2):

Table 2. 102 Series propeller dimensions and specifications.

No. blades	4
Rotation	R.H.
D (m)	0.3048
Pitch	0.8
B.A.R	0.85
Material	Stone Manganese

In contrast to tidal turbines, the governing equations regarding propellers and their hydrodynamic particulars are the following:

$$J = \frac{V_a}{nD} \tag{5}$$

$$K_T = \frac{T}{\rho n^2 D^4} \tag{6}$$

$$K_Q = \frac{Q}{\rho n^2 D^5} \tag{7}$$

Further below, the curves that were produced during the past experiments on the 102 series propeller, were reused for the present tests to make a comparison between them. In this test, the shaft rotational speed was fixed at 800 RPM (rps = 13).

In Figure 15, the K_T and $10K_Q$ curves are shown, which agree well in terms of the trend of the curves. However, since the test matrix used for both tests in the past and present was the same, the curves should have coincided with each other. The curves have an approximate error of 5%, which is enough to consider that the performance of the dynamometer deteriorated, making it unable to produce perfect results. The results of the tests on the propeller proved that the key problem of the H45 dyno was its accuracy and reliability, even though the measured values were well suited for the capacity of the dynamometer. We also noted that both the current study's measurements and the previous study's measurements had the same problem, i.e., the dynamometer produced unreliable data and fluctuations when both torque and thrust values were small. This is an abnormal characteristic for a dynamometer, which means that the dynamometer has had this problem since 40 years ago. As the very small torque and thrust values did not fall into practical application range (i.e., J greater than 0.65 for a propeller with a pitch ratio of 0.8), the majority of the measurements are still acceptable.

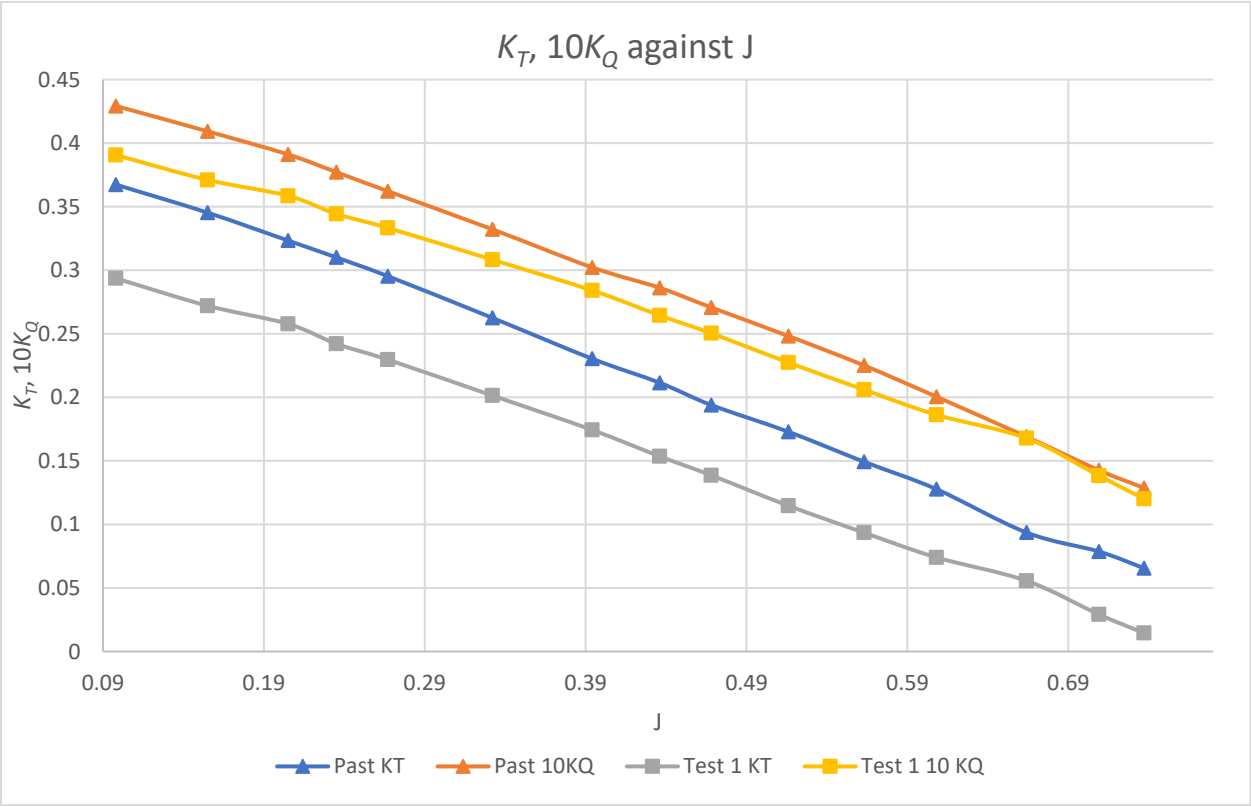

Figure 15. K_T and $10K_Q$ against J comparison between past and present data.

3.3. Numerical Prediction

In this section, an in-house code, Rotorysics (formerly Propella [25–27]), was used to perform cavitation prediction based on the test matrix that could not be completed experimentally, especially for the low cavitation numbers where the required vacuum level could not be sufficiently applied. The code is based on the panel method, similar to UAEARO that was developed by Analytical Method Inc. [28] and PMARC by NASA Ames Research Center [29]. Propella was developed by Liu, specifically for rotor wing aero- and hydrodynamics performance evaluations [26,27,30].

3.3.1. Numerical Cavitation Prediction

The code used for the acquisition of numerical data has been proven in the past to produce accurate and reliable cavitation prediction [31], with resultant thrust and torque coefficients from experimental tests and numerical tests using the code being exceptionally

close. The code was used particularly for predicting the effects of sheet cavitation on the propulsive performance of propellers and tidal turbines, which is the main cause that degrades their performance [32,33]. Table 3 lists the test condition as part of the test matrix.

Table 3. Example test matrix for J = 0.785 or TSR = 4.

TSR = 4		
SIGMA_N	**C_T**	**C_{pow}**
0.5	0.0031	0.04584
1	0.192565	0.077511
1.5	0.340111	0.194666
2	0.416289	0.257854
2.5	0.464931	0.297481
3	0.495928	0.322021
5	0.521846	0.341059
7	0.68696	0.343881

Upon completing the code test runs for each tidal turbine, the following curves were produced for thrust/drag coefficient C_T and power coefficient C_{pow} against cavitation number σ_n, which are important to assess the effect of cavitation on the performance of the tidal turbines for a given TSR value, as shown in Figures 16–19.

As seen through Figures 16–19, the effect of cavitation on the thrust/drag coefficient and torque coefficient was quite severe, as the lower the cavitation number, the lower their magnitudes. As soon as the cavitation number advanced close to 3, the coefficients of both tidal turbines improved dramatically. Beyond the point of σ_n = 3, the curves begin to slightly increase until they reach their optimum point, which is the area between cavitation numbers 3–7. Then, between cavitation numbers 5–7, the coefficients start to reach a slight steady-state point.

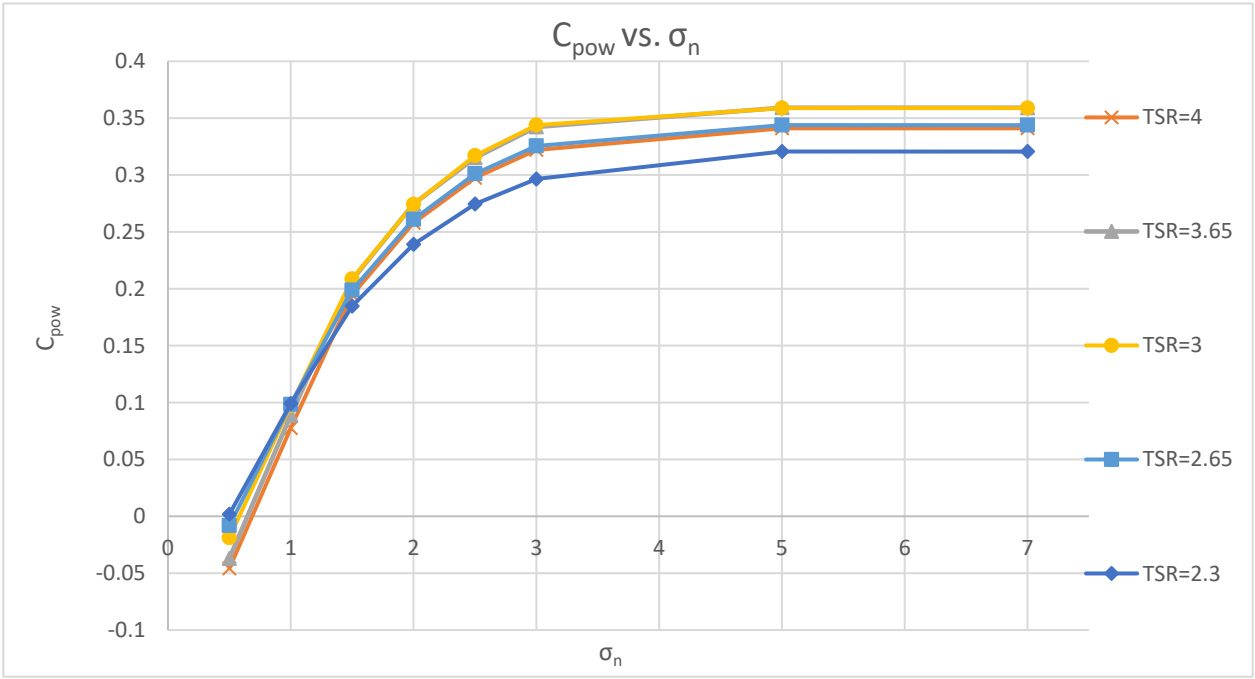

Figure 16. Zero-degree skewness tidal turbine, C_{pow} vs. σ_n.

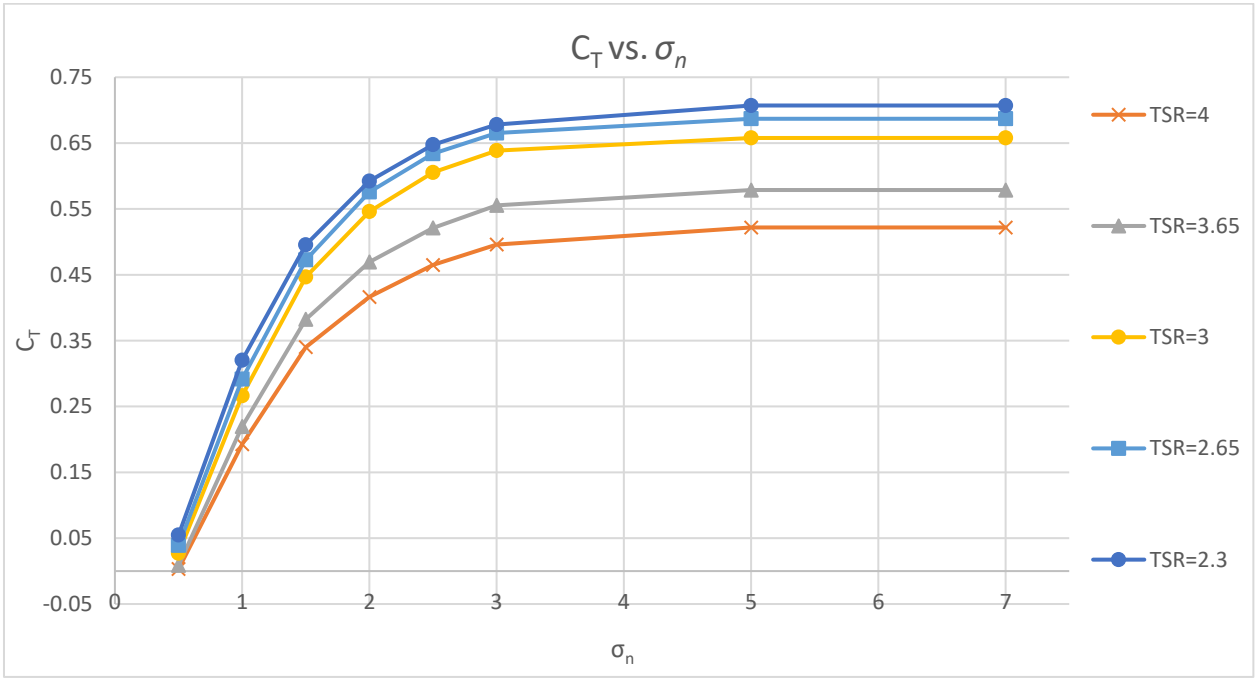

Figure 17. Zero-degree skewness tidal turbine, C_T vs. σ_n.

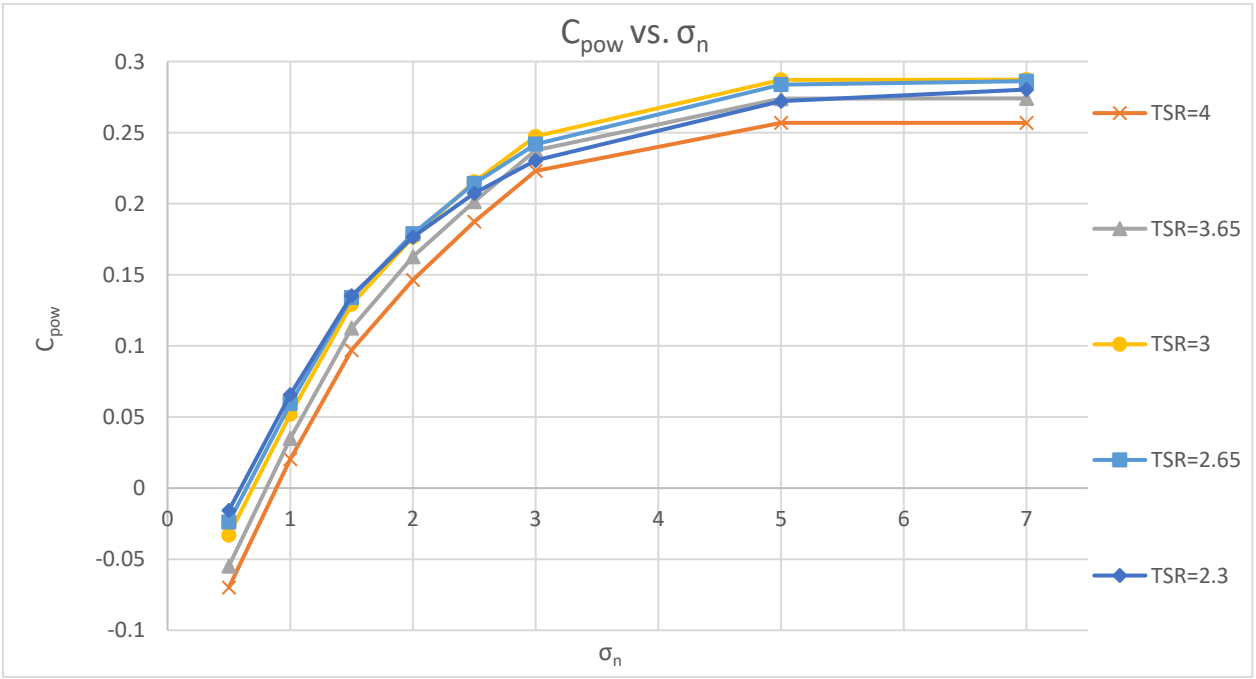

Figure 18. Ninety-degree skewness tidal turbine, C_{pow} vs. σ_n.

It is evident that in terms of the power coefficient, the 0 degree-skewed tidal rotor had the highest efficiency, which was around 0.36 at a TSR value of 3.65 and $\sigma_n = 5$, compared to the positive 90-degree skewed rotor that had a maximum power coefficient of 0.29 at a TSR of 3 and $\sigma_n = 7$. On the other hand, the maximum thrust/drag coefficient for both tidal rotors were almost equal.

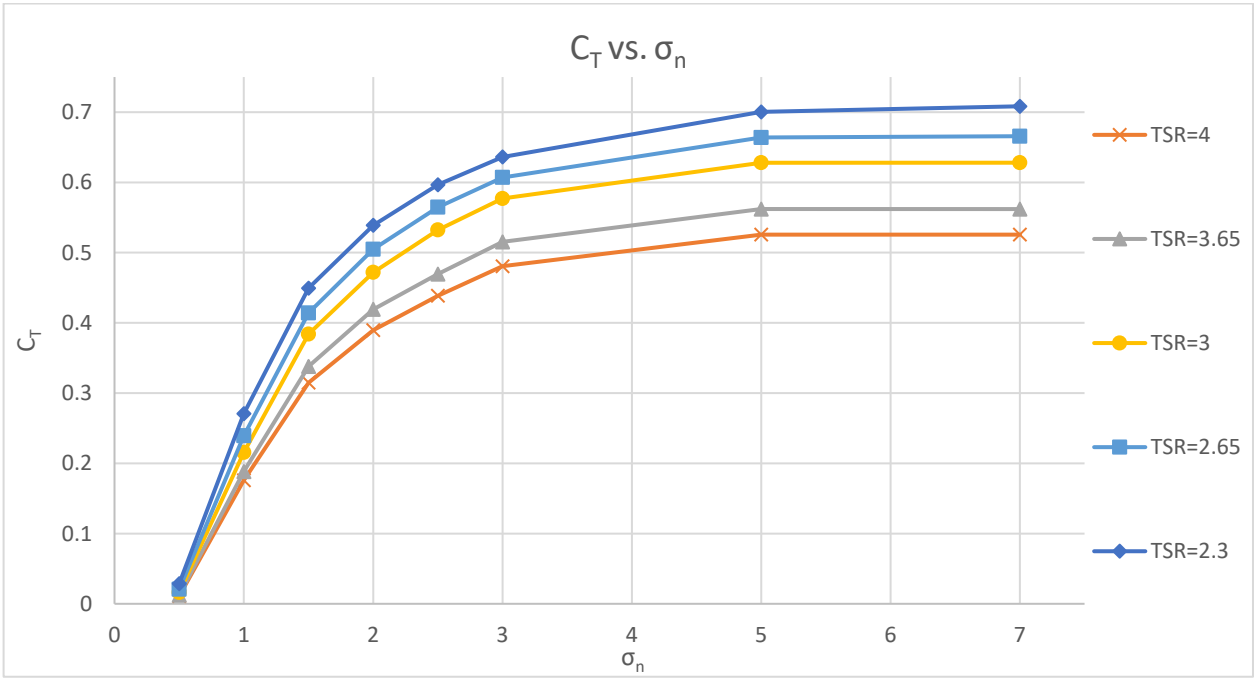

Figure 19. Ninety-degree skewness tidal turbine, C_T vs. σ_n.

3.3.2. Numerical Open Water Test Prediction

The same process was repeated to obtain the numerical results for the open water test conditions, without cavitation. This was simulated using a high cavitation number (around 7), where the effects of cavitation are non-existent. The results of the comparison between the 0 degree-skewed (R0) and positive 90 degree-skewed tidal turbines are presented while using the same test matrix as in Appendix A Table A4, as shown Figures 20 and 21.

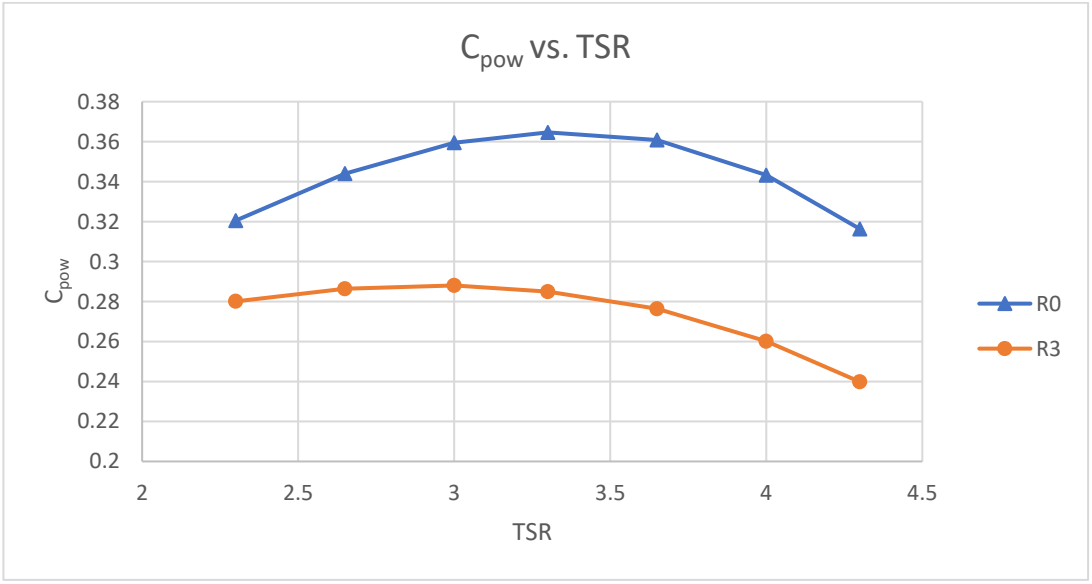

Figure 20. Open water test, C_{pow} vs. TSR.

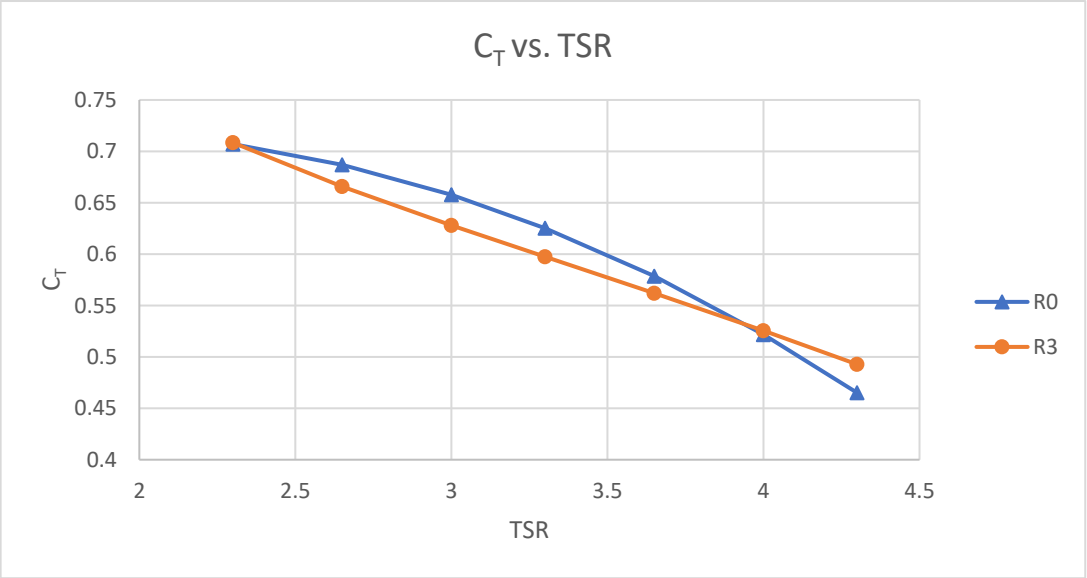

Figure 21. Open water test, C_T vs. TSR.

The open water test was used to see how much the effect of the rotor blade skew on power production performance was. In terms of power coefficients, i.e., the power production performance, these predicted values under open water condition were actually the same as in the cavitation at a large enough cavitation number (i.e., $\sigma_n \geq 7$). It can be seen that the R0 rotor (zero-skew) had the highest efficiency at every value of TSR compared to the R3 rotor (the highest skew of 90 degrees), while its optimum point occurred at a TSR value of 3.3. Conversely, the R3 rotor had a slightly higher drag/thrust coefficient at a TSR value of 2.3, but this did not affect the power production coefficient because for most tidal turbines, when placed deep enough, cavitation is no longer a concern. Again, it can be seen that the rotor R0 is much more efficient than the R3 rotor in terms of power production efficiency. The reason for the lower skewed turbine having higher power production efficiency is due to the increase in the equivalent blade area, and hence the total friction, which mostly contributes to the increased torque (i.e., the input power), resulting in a lower efficiency.

3.3.3. Experimental and Numerical Cavitation Test Comparison

A comparison between the experimental and numerical cavitation data is presented for the zero-skew rotor (R0), for a fixed TSR value of 2.3. Once again, the code was used to replicate the same experimental conditions and parameters.

As observed from Figure 22, the curve of the experimental data obtained through the cavitation tests is similar to the ideal one, as depicted by the numerical curve.

In general, there was a difference in magnitude between the experimental and numerical data, which could be traced back to the dynamometer issue. The experimental curve had some abnormal values, especially for the low cavitation number range; however, since tidal turbines, in contrast to propellers, operate at high cavitation numbers, cavitation and its effects on the operation and performance of the tidal turbines, is negligible.

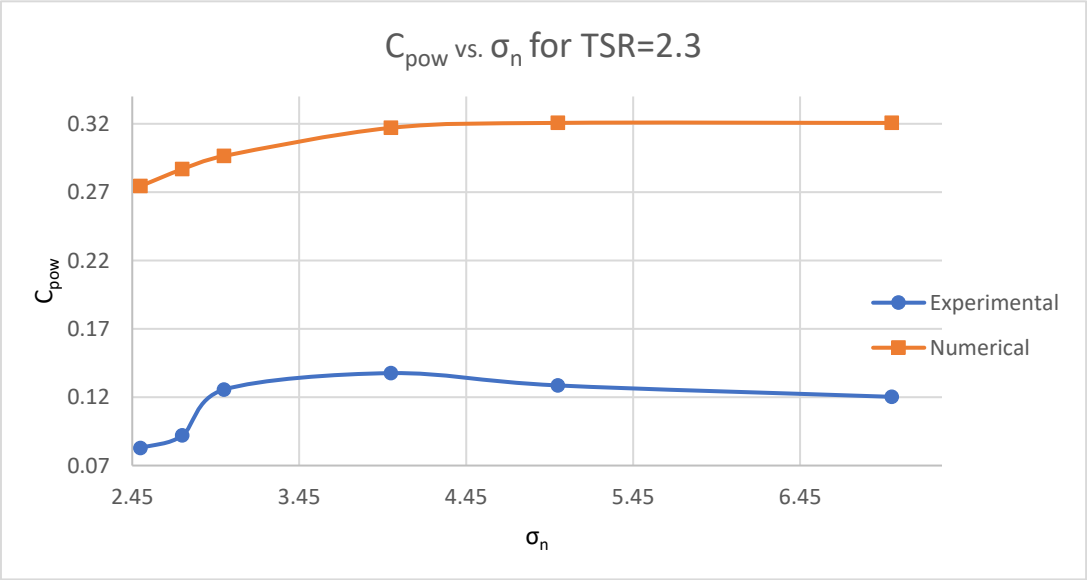

Figure 22. Experimental and numerical C_{pow} vs. σ_n for TSR = 2.3.

4. Conclusions and Recommendations

There have been few studies conducted on highly skewed turbines in the literature. This study is one of the pioneering attempts to obtain the effect of highly skewed tidal turbine rotors on their energy production efficiency. Two rotors, 0-degree- and positive 90-degree-skewed rotors made of stainless steel 316L, were 3-D printed using a laser powder bed fusion technique. Three key research questions were addressed: 1. The effect of highly skewed blades on the hydrodynamic performance of turbine rotors; 2. The effect of materials on hydrodynamic performance between plastic 3-D printed rotors and stainless steel 3-D printed rotors; 3. The highly skewed rotor effect on cavitation.

The propeller dynamometer H45 used for experiments was found to have substantial discrepancies compared to its measurements when it was new. The dynamometer also had some problems in very low load cases when it was newly installed, as indicated by the results of the comparison analysis. A new dynamometer and mounting assembly has been designed and is being fabricated to replace the current H45 dynamometer. As the key research questions related to cavitation on highly skewed horizontal axis turbine rotors, a robust and reliable software code was used to make sure the research questions were addressed.

The effect of cavitation on the thrust/drag coefficient and torque coefficient is severe, as the lower the cavitation number, the lower their magnitudes. As soon as the cavitation number advanced close to 3, the coefficients of both tidal turbines improved dramatically. Beyond the point of $\sigma_n = 3$, the curves began to slightly increase until they reached their optimum point, which was the area between cavitation numbers 3–7. Then, between cavitation numbers 5–7, the coefficients began to reach a slight steady-state point.

In terms of the power coefficient, the 0-degree-skewed tidal rotor had the highest efficiency, which was around 0.36 at a TSR value of 3.65 and $\sigma_n = 5$, compared to the positive 90-degree-skewed rotor that had a maximum power coefficient of 0.29 at a TSR of 3 and $\sigma_n = 7$; this means that the highest optimum power coefficient location at this TSR value had a shift due to the skew. For the 90-degree, the largest practical skew arguably produced a substantially large sacrifice in power production. This sacrifice in power generation is substantial, thus a relatively smaller skew between 0 and 90 degrees was determined in practice to produce a balanced power production efficiency and level of blade skew, for any particular situation in practice. These results and findings, along with the conclusions, will serve tidal turbine designers and researchers for the trade-off of power production performance with reduced cavitation and underwater noise.

Author Contributions: Conceptualization, P.L.; methodology, P.L., S.A.P., S.T. (Sravya Tekumalla), A.S., S.T. (Serkan Turkmen) and W.L.E.W.; software, P.L.; validation, P.L., S.A.P. and S.T. (Serkan Turkmen); formal analysis, S.A.P. and P.L.; investigation, S.A.P.; resources, S.T. (Serkan Turkmen); data curation, S.A.P.; writing—original draft preparation, S.A.P.; writing—review and editing, P.L., S.T. (Sravya Tekumalla), A.S., W.L.E.W.; visualization, S.A.P. and P.L.; supervision, P.L. and S.T. (Serkan Turkmen); project administration, P.L.; funding acquisition, P.L. and S.T. (Sravya Tekumalla). All authors have read and agreed to the published version of the manuscript.

Funding: NTU Presidential Postdoctoral Fellowship for S. Tekumalla and Newcastle University Start-up funding for P.L.

Data Availability Statement: The research data of this project is available upon request.

Acknowledgments: The authors thank Newcastle University for its support. The authors would also like to acknowledge Additive Industries Asia Pacific Pte. Ltd., Singapore, for their support with printing the tidal turbine rotors.

Conflicts of Interest: The authors declare no conflict of interest.

Nomenclature

Notation	Description	Units
A	Rotor sweep area	m^2
Ω	Shaft revolution speed	rad/s
P_{shaft}	Shaft pressure	Pa
ρ	Water density	kg/m^3
V_a	Inflow velocity	m/s
D	Diameter of rotor	m
Q	Rotor shaft torque	Nm
T	Thrust	N
R	Rotor radius	m
n	Rotor shaft speed, revolutions per second	rps
ω	Rotor shaft speed, radians per second	rad/s
TSR	Dimensionless tip speed ratio $TSR = \omega R/V_a$	
C_{pow}	Power coefficient $C_{pow} = Q_{torque}\omega/0.5\rho {V_a}^3 A$	
C_t	Thrust coefficient $C_t = T_{thrust}/0.5\rho {V_a}^2 A$	
K_T	Thrust coefficient for propellers $K_t = T_{thrust}/\rho n^2 D^4$	
K_Q	Torque coefficient for propellers $K_q = Q_{torque}/\rho n^2 D^5$	
σ_n	Cavitation number $\sigma_n = (P_{shaft} - P_{vapour})/0.5\rho n^2 D^2$	
P_{atm}	Atmospheric pressure	Pa
P_{vapour}	Vapor pressure	Pa
G	Acceleration of gravity	m/s^2
H	Shaft immersion depth	m
J	Advance coefficient$J = V_a/nD$	

Appendix A

Table A1. Test matrix for open water test No.5.

TSR	V_a (m/s)	Dial Reading	Thrust (N)	Torque (Nm)	C_T	Power (W)	C_{pow}
2.3	4.10	6.17	28.13955	2.189464	0.047502	137.5681	0.0566715
2.65	3.56	5.36	28.76455	2.189924	0.064459	137.597	0.086698195
3	3.14	4.73	27.82161	2.159887	0.079902	135.7097	0.124061831
3.3	2.86	4.30	28.56014	2.167888	0.099248	136.2124	0.165737985
3.65	2.58	3.88	29.43748	2.173822	0.125147	136.5853	0.22487748
4	2.36	3.54	30.10154	2.179382	0.153689	136.9346	0.296726768
4.3	2.19	3.29	29.84755	2.164305	0.176108	135.9873	0.366072599

Table A2. Experimental test matrix based on previous study.

TSR	rps	RPM	V_a (m/s)	Dial V Reading (m/s)	Thrust (N)	Torque (Nm)	C_T	Power (W)	C_{pow}
2.3	5	300	2.048865	3.1	109.693	3.220744	0.74068	101.1827	0.33346
2.65	6	360	2.133912	3.2	111.559	3.079477	0.69443	116.0935	0.338653
3	7	420	2.199115	3.3	112.176	2.977494	0.65748	130.9638	0.349048
3.3	7	420	1.999195	3.0	85.9881	2.364039	0.60982	103.9813	0.368864
3.65	8	480	2.065705	3.1	81.3263	2.123111	0.54022	106.7247	0.343192
4	8	480	1.884956	2.8	57.1588	1.601265	0.45599	80.49254	0.340666
4.3	8	480	1.753447	2.6	43.3048	1.289615	0.39923	64.82649	0.340841

Table A3. Modified test matrix with 2x increased rps and V_a.

TSR	rps	RPM	V_a (m/s)	Dial V Reading (m/s)	Thrust (N)	Torque (Nm)	C_T	Power (W)	C_{pow}
2.3	10	600	4.0977295	6.2	489.1468	10.960017	0.825714	688.6382	0.283686
2.65	12	720	4.267824	6.4	485.3466	10.154839	0.755294	765.6966	0.279199
3	14	840	4.3982297	6.6	473.7707	9.179611	0.694207	807.5228	0.269028
3.3	14	840	3.9983907	6.0	365.5981	6.650146	0.648202	585.0078	0.259408
3.65	16	960	4.1314095	6.2	349.756	5.660978	0.580825	569.1332	0.228768
4	16	960	3.7699112	5.7	267.8841	3.845839	0.534271	386.646	0.204549
4.3	16	960	3.5068941	5.3	204.4442	2.457122	0.471201	247.0297	0.162352

Table A4. Final modified test matrix.

TSR	rps	RPM	V_a (m/s)	Dial V Reading (m/s)	Thrust (N)	Torque (Nm)	C_T	Power (W)	C_{pow}
2.3	12.5	750	5.1221619	7.7	720.9716	16.672119	0.778912	1309.425	0.276183
2.65	15	900	5.33478	8.0	719.1454	15.664198	0.716243	1476.393	0.275632
3	17.5	1050	5.4977871	8.3	710.217	14.451534	0.666027	1589.112	0.271061
3.3	17.5	1050	4.9979883	7.5	548.3886	10.401082	0.622264	1143.718	0.259663
3.65	20	1200	5.1642619	7.8	541.385	9.284235	0.575396	1166.752	0.240121
4	20	1200	4.712389	7.1	398.3702	6.091844	0.508489	765.5635	0.207365
4.3	20	1200	4.3836177	6.6	308.9487	4.179566	0.45572	525.2471	0.176743

Table A5. Example test run 21.

TSR	rps	RPM	V_a (m/s)	Dial V Reading (m/s)	Thrust (N)	Torque (Nm)	C_T	Power (W)	C_{pow}
2.3	14	840	5.7368214	8.6	864.551	20.082297	0.744603	1766.531	0.265207
2.65	14	840	4.979128	7.5	621.331	13.566333	0.710384	1193.357	0.274023
3	14	840	4.3982297	6.6	448.3187	9.236368	0.656913	812.4734	0.270678
3.3	14	840	3.9983907	6.0	341.3479	6.809696	0.605207	599.0121	0.265618
3.65	14	840	3.6149833	5.4	248.1309	4.699654	0.538202	413.4032	0.248046
4	14	840	3.2986723	5.0	192.3474	3.478906	0.501054	306.0206	0.241663
4.3	14	840	3.0685324	4.6	142.8248	2.415297	0.429951	212.4606	0.208431

Table A6. Past experiment test matrix.

J	V_a (m/s)	Dial Reading (m/s)	Thrust (N)	Torque (Nm)	K_T	K_Q	$10K_Q$
0.098	0.398272	0.59	562.7	20.04	0.367382862	0.042926426	0.429264261
0.155	0.62992	0.94	528.9	19.11	0.34531508	0.040934332	0.409343315
0.205	0.83312	1.24	495.3	18.26	0.323377877	0.0391136	0.391135999
0.235	0.95504	1.43	475	17.61	0.310124151	0.037721276	0.377212757
0.267	1.085088	1.62	452.4	16.91	0.29536877	0.03622185	0.362218496
0.332	1.349248	2.02	402.1	15.51	0.262528255	0.033222997	0.332229975
0.394	1.601216	2.40	352.9	14.11	0.230405922	0.030224145	0.302241453
0.436	1.771904	2.66	323.9	13.36	0.211472026	0.028617617	0.286176174
0.468	1.901952	2.86	297.1	12.64	0.193974495	0.027075351	0.270753506
0.516	2.097024	3.15	264.8	11.59	0.172886053	0.024826212	0.248262115
0.563	2.288032	3.44	228.7	10.51	0.149316617	0.022512811	0.225128113
0.608	2.470912	3.72	195.7	9.36	0.12777115	0.020049468	0.200494685
0.664	2.698496	4.06	143.4	7.89	0.093624849	0.016900674	0.169006738
0.709	2.881376	4.34	120.5	6.66	0.0786736	0.014265968	0.14265968
0.737	2.995168	4.51	100.5	6.01	0.065615741	0.012873644	0.128736438

Table A7. Cavitation test, test matrix.

Cn	Thrust (N)	Torque (Nm)	C_T	Power (W)	C_{pow}	P_{tunnel} (Pa)	P_{tunnel} Needed (inhg)
2.5	315.8421	6.270059	0.0054	551.5432	0.082802	−81,275	−24.00050345
2.75	333.2402	6.968916	0.006002	613.0179	0.092031	−79,073.9	−23.35053431
3	383.2106	9.507302	0.008188	836.306	0.125553	−76,872.9	−22.70056517
4	414.0965	10.42007	0.008974	916.5975	0.137607	−68,068.7	−20.1006886
5	431.6688	9.738093	0.008387	856.6074	0.128601	−59,264.5	−17.50081203
7	451.5683	9.107689	0.007844	801.1542	0.120276	−41,656.1	−12.30105889

Appendix B

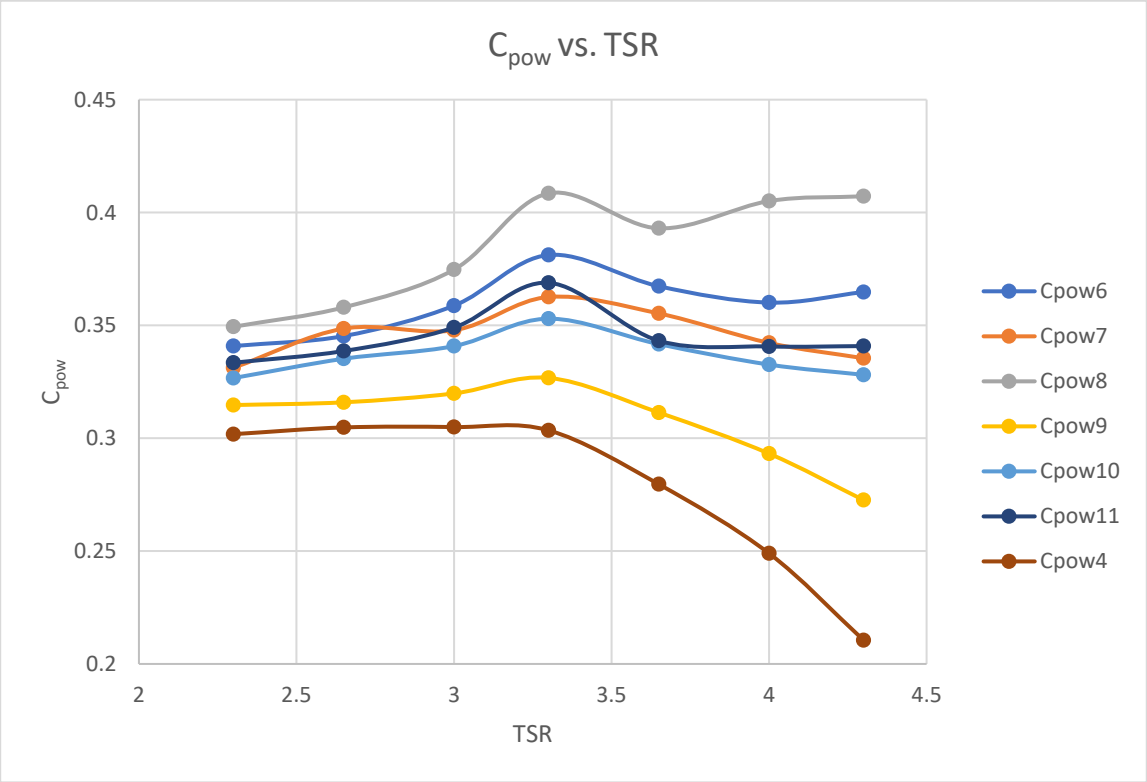

Figure A1. C_{pow} vs. TSR test matrix (the same test matrix as that of Foong, 2019), cavitation tunnel results.

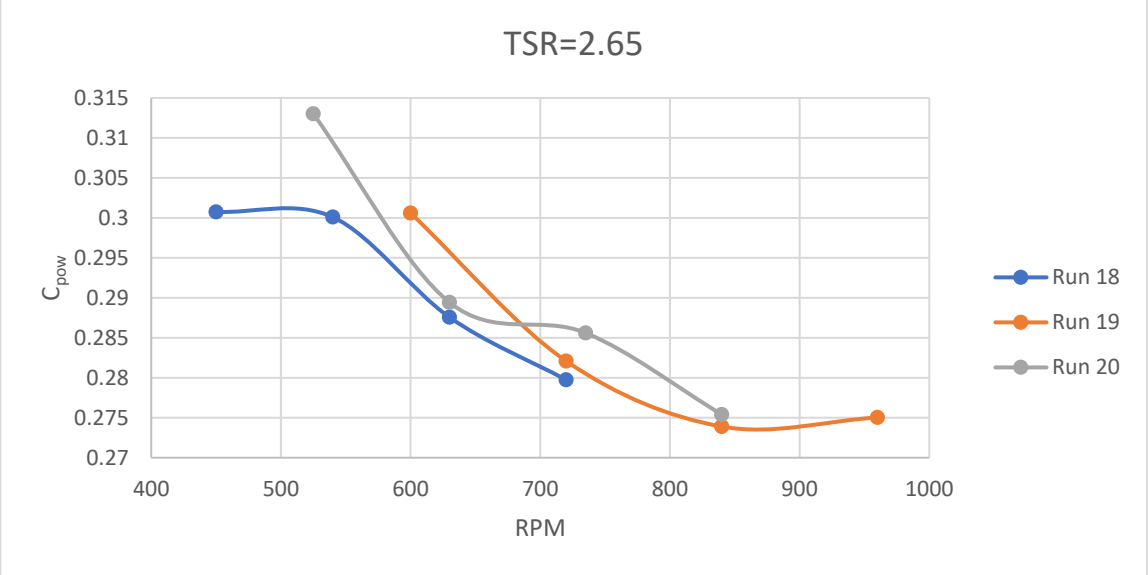

Figure A2. Constant TSR, C_{pow} comparison.

References

1. Feliciano, D. *Net Zero: The UK's Contribution to Stopping Global Warming Committee on Climate Change*; University of Edinburgh: Edinburgh, UK, 2019.
2. Zobaa, A.; Bansal, R. *Handbook of Renewable Energy Technology*; World Scientific: Singapore, 2011.
3. Singla, S. Effects of Noise Pollution from Ships on Marine Life. *Mar. Insight* **2019**, 367–389.
4. Farcas, A.; Thompson, P.M.; Merchant, N.D. Underwater Noise Modelling for Environmental Impact Assessment. *Environ. Impact Assess. Rev.* **2016**, *57*, 114–122. [CrossRef]
5. Kumar, A.; Das, T.K.; Samad, A. Effect of Blade Skew, Endplate and Casing Groove on the Aerodynamic Performance of Wells Turbine for OWC: A Review. *J. Phys. Conf. Ser.* **2022**, *2217*, 012070. [CrossRef]
6. Magagna, D. Wave and Tidal Energy Strategic Technology Agenda. *Si Ocean* **2014**, *44*, 1–44.
7. Harrold, M.; Ouro, P. Rotor Loading Characteristics of a Full-Scale Tidal Turbine. *Energies* **2019**, *12*, 1035. [CrossRef]
8. Asnaghi, A.; Svennberg, U.; Bensow, R.E. Numerical and Experimental Analysis of Cavitation Inception Behaviour for High-Skewed Low-Noise Propellers. *Appl. Ocean Res.* **2018**, *79*, 197–214. [CrossRef]
9. Tong, X.D.; Chen, H.Y.; Chen, Y. Low Frequency Broadband Noise Radiated by Highly Skewed Propeller Ingesting Inflow Turbulence. *J. Sound Vib.* **2021**, *490*, 115709. [CrossRef]
10. Ebrahimi, A.; Razaghian, A.H.; Tootian, A.; Seif, M.S. An Experimental Investigation of Hydrodynamic Performance, Cavitation, and Noise of a Normal Skew B-Series Marine Propeller in the Cavitation Tunnel. *Ocean Eng.* **2021**, *238*, 109739. [CrossRef]
11. Yu, K.; Park, D.; Choi, J.; Seol, H.; Park, I.; Lee, S. Effect of Skew on the Tonal Noise Characteristics of a Full-Scale Submarine Propeller. *Ocean Eng.* **2023**, *276*, 114218. [CrossRef]
12. Hadipour, A.; Abadi, K.A.V.; Khanzadi, H.; Motahari, H. Hydrodynamic Analysis of Noise Propagation by the High Skew Marine Propeller Working in Non-uniform Inflow. *Int. J. Appl. Mech. Eng.* **2021**, *26*, 104–121. [CrossRef]
13. Lippert, R. *Numerical Models to Simulate Underwater Turbine Noise Levels*; Florida Atlantic University: Boca Raton, FL, USA, 2012.
14. Muller, P.; Pécot, F. Development of a Fluid Structure Coupling For Composite Tidal Turbines and Marine Propellers. In Proceedings of the VII International Conference on Computational Methods in Marine Engineering CIMNE, Nantes, France, 15–17 May 2017; pp. 635–646.
15. Starzmann, R.; Carolus, T. Effect of Blade Skew Strategies on the Operating Range and Aeroacoustic Performance of the Wells Turbine. *J. Turbomach.* **2014**, *136*, 011003. [CrossRef]
16. Ge, M.; Manikkam, P.; Ghossein, J.; Subramanian, R.K.; Coutier-Delgosha, O.; Zhang, G. Dynamic Mode Decomposition to Classify Cavitating Flow Regimes Induced by Thermodynamic Effects. *Energy* **2022**, *254*, 124426. [CrossRef]
17. Ge, M.; Sun, C.; Zhang, G.; Coutier-Delgosha, O.; Fan, D. Combined Suppression Effects on Hydrodynamic Cavitation Performance in Venturi-Type Reactor for Process Intensification. *Ultrason. Sonochem.* **2022**, *86*, 106035. [CrossRef] [PubMed]
18. Cooper, N.; Grimwade, J.; Rowe, S.; Langston, D. Whitby Pier Power. In *Innovative Coastal Zone Management: Sustainable Engineering for a Dynamic Coast*; ICE Publishing: London, UK, 2012; pp. 96–103.
19. Batten, W.M.J.; Bahaj, A.S.; Molland, A.F.; Chaplin, J.R. The prediction of the hydrodynamic performance of marine current turbines. *Renew. Energy* **2008**, *33*, 1085–1096. [CrossRef]
20. Magagna, D.; Uihlein, A. Ocean Energy Development in Europe: Current Status and Future Perspectives. *Int. J. Mar. Energy* **2015**, *11*, 84–104. [CrossRef]

21. Foong, J.M. Hydrodynamic Effect of Highly Skewed Horizontal Axis Tidal Turbine (HATT) Rotor. Bachelor's Dissertation, Australian Maritime College, University of Tasmania, Launceston, TAS, Australia, 2019.
22. Krasilnikov, V.; Sileo, L.; Joung, T.-H. Investigation into the Influence of Reynolds Number on Open Water Characteristics of Pod Propulsors. In Proceedings of the International Symposiums on Marine Propulsors, Austin, TX, USA, 31 May–4 June 2015.
23. ITTC Quality Manual as Procedure 7.5-02-03-02.1. 2014. Available online: https://www.ittc.info/media/8025/75-02-03-021.pdf (accessed on 1 March 2023).
24. International Towing Tank Conference. *Testing and Data Analysis*; International Towing Tank Conference: Fukuoka, Japan, 2008.
25. Liu, P. Rotorysics User Manual. 2019; 50.
26. Liu, P. *Software Development on Propeller Geometry Input Processing and Panel Method Predictions of Propulsive Performance of the R-Class Propeller TDC Contract Report*; Ocean Engineering Research Centre: St, John's, NL, Canada, 1996.
27. Liu, P.; Bose, N. An Unsteady Panel Method for Highly Skewed Propellers in Non-uniform Inflow. In Proceedings of the Propeller RANS/Panel Method Workshop (ITTC), Grenoble, France, 5–6 April 1998; pp. 343–350.
28. Maskew, B. Prediction of Subsonic Aerodynamic Characteristics: A Case for Low-Order Panel Methods. *J. Aircraft* **1982**, *19*, 157–163. [CrossRef]
29. Lambert, M.; Platzer, M. Evaluation of the Nasa-Ames Panel Method (Pmarc) For Aerodynamic Missile Design. In Proceedings of the 34th Aerospace Sciences Meeting and Exhibit, Reno, NV, USA, 15–18 January 1995; p. 775.
30. Liu, P.; Bose, N. Rototyping a Series of Bi-directional Horizontal Axis Tidal Turbines for Optimum Energy Conversion. *Appl. Energy* **2012**, *99*, 50–66. [CrossRef]
31. Liu, P. *Marine Propeller and Turbine Rotor Prototyping, Design and Optimization*; Thomas Nelson: Edinburgh, UK, 2020; ISBN 978-1-8383505-0-5.
32. Liu, P.; Bose, N.; Colbourne, B. Incorporation of a Critical Pressure Scheme into a Time-Domain Panel Method for Propeller Sheet Cavitation. In Proceedings of the International Workshop on Ship Hydrodynamics (IWSH2001), Wuhan, China, 22–26 September 2001.
33. Islam, M.F.; Veitch, B.; Liu, P. Experimental Research on Marine Podded Propulsors. *J. Nav. Archit. Mar. Eng.* **2007**, *4*, 57–71. [CrossRef]